6670 *Inorg. Chem.* **2009**, *48*, 6670–6679
DOI: 10.1021/ic900634t

Inorganic Chemistry
Article

Iron(II) Tris-[N^4-substituted-3,5-di(2-pyridyl)-1,2,4-triazole] Complexes: Structural, Magnetic, NMR, and Density Functional Theory Studies

Jonathan A. Kitchen,[†] Nicholas G. White,[†] Maruta Boyd,[‡] Boujemaa Moubaraki,[§] Keith S. Murray,[§] Peter D. W. Boyd,[∥] and Sally Brooker*[,†]

[†]*Department of Chemistry and The MacDiarmid Institute for Advanced Materials and Nanotechnology, University of Otago, P.O. Box 56, Dunedin, New Zealand,* [‡]*Auckland Cancer Society Research Centre, Faculty of Medicine and Health Science, University of Auckland, Private Bag 92019, Auckland, New Zealand,* [§]*School of Chemistry, Building 23, Monash University, Clayton, Victoria 3800, Australia, and* [∥]*Department of Chemistry, The University of Auckland, Private Bag 92019, Auckland, New Zealand*

Received March 31, 2009

Eight mononuclear iron(II) complexes of N^4-3,5-di(2-pyridyl)-1,2,4-triazole (**Rdpt**) ligands have been prepared and characterized. In all cases the iron(II)/ligand ratio used is 1:3, giving red complexes of the general formula $[Fe^{II}(\mathbf{Rdpt})_3](BF_4)_2 \cdot solvents$, in 55−89% yield. The ligands differ only in the nature of the N^4-substituent (amino, pyrrolyl, *iso*-butyl, methyl, phenyl, *para*-tolyl, 3,5-dichlorophenyl, and 4-pyridyl; for ligands **adpt**, **pldpt**, **ibdpt**, **medpt**, **phdpt**, **ptdpt**, **Cldpt**, and **pydpt**, respectively) allowing substituent effects on the properties of the resulting iron(II) complexes to be probed. The low temperature crystal structures of seven of the complexes reveal low spin iron(II) environments. Packing analyses reveal anion-π and acetonitrile-π interactions involving the tetrafluoroborate counteranions and interstitial acetonitrile molecules, respectively. Both "π-pockets" and "π-sandwiches" are observed. Solid state magnetic susceptibility measurements (4−300 K) indicate the iron(II) is low spin (LS) in all complexes at all temperatures studied, except for $[Fe^{II}(\mathbf{pldpt})_3](BF_4)_2 \cdot 1^1/_2H_2O$ which has the beginnings of spin crossover (SCO) at elevated temperatures. Downfield shifts and peak broadening observed in the variable temperature ^{1}H NMR studies indicate that in d_3-nitromethane solution the LS $[Fe^{II}(\mathbf{Rdpt})_3]^{2+}$ complexes are in equilibrium with a trace of a high spin (HS) species. ^{15}N NMR spectra (measured and calculated) of the ligands reveal that altering the N^4-substituent changes the chemical shift of the N^1 triazole and pyridine nitrogen atoms, allowing probing of the relationship between ligand substituent and the nature of the coordinating nitrogen atoms.

Introduction

The use of the 1,2,4-triazole moiety in iron(II) spin crossover (SCO) complexes has been well documented.[1−4] The ligand field strength of such triazole-based ligands often lies in the right region to facilitate temperature mediated switching between the high spin (HS) and low spin (LS) states of the iron(II) centers.[2] This bistability gives rise to the possibility of applications in nanotechnology.[5,6] Certain requirements must be met for such complexes to be viable nanocomponents. Ideally the transition between spin states should be abrupt and occur with a hysteresis loop which is centered around room temperature. Many complexes that display these properties are polynuclear as a triazole bridging two metal centers through N^1 and N^2 results in strong cooperativity between the iron(II) centers, allowing the passing on of the information about a spin state change and hence an abrupt SCO, possibly with hysteresis.[3,5] In mononuclear complexes any interactions between the metal centers are facilitated by weaker interactions, such as hydrogen bonding and $\pi-\pi$ stacking, and is often mediated and/or moderated by solvent molecules of crystallization and/or the counterion(s). Hence SCO is often, but certainly not always, gradual and without hysteresis in mononuclear complexes.

We have developed a reliable and general route to our choice of the N^4-substituent in symmetric N^4-substituted-3,5-di(2-pyridyl)-4*H*-1,2,4-triazoles (**Rdpt**, Figure 1) and asymmetric N^4-substituted-3-(2-pyridyl)-5-(phenyl)-4*H*-1,2,4-triazoles.[7] The **Rdpt** ligands studied to date have been

*To whom correspondence should be addressed. E-mail: sbrooker@chemistry.otago.ac.nz.

(1) (a) Haasnoot, J. G. *1,2,4-Triazoles as ligands for iron(II) high spin-low spin crossovers*; Kluwer Academic Publishers: Dordrecht, 1996; p 299−321; (b) Lavrenova, L. G.; Larionov, S. V. Russ. J. Coord. Chem. 1998, 24, 379–395.
(2) (a) Kahn, O.; Codjovi, E. *Philos. Trans. R. Soc., A* **1996**, *354*, 359–379. (b) van Koningsbruggen, P. J. *Top. Curr. Chem.* **2004**, *233*, 123–149.
(3) Kahn, O. *Chem. Ber.* **1999**, *2*, 24–27.
(4) Kitchen, J. A.; Brooker, S. *Coord. Chem. Rev.* **2008**, *252*, 2072–2092.
(5) Kahn, O.; Martinez, C. J. *Science (Washington, D.C.)* **1998**, *279*, 44–48.
(6) Letard, J.-F.; Guionneau, P.; Capes, L. *Top. Curr. Chem.* **2004**, *235*, 221–249.
(7) Klingele, M. H.; Brooker, S. *Eur. J. Org. Chem.* **2004**, 3422–3434.

 Published on Web 06/17/2009

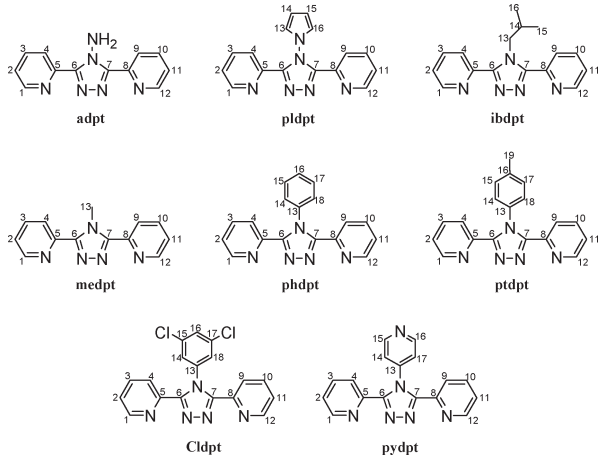

Figure 1. Di-pyridyl-triazole ligands, **Rdpt**, used in this study.

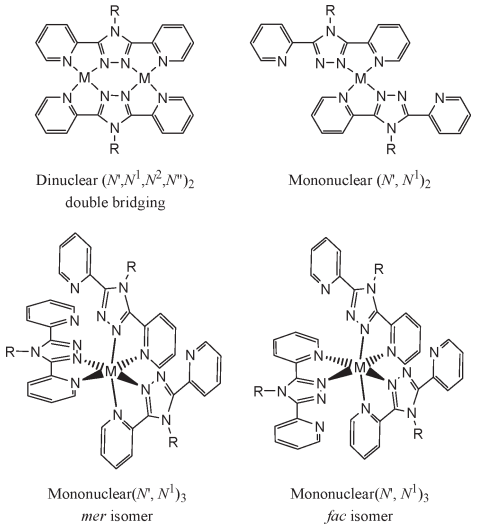

Figure 2. Some possible binding modes of di-pyridyl-triazole, **Rdpt**, ligands.

documented to produce both dinuclear (N',N^1,N^2,N'')$_2$ double bridging complexes, $[M_2^{II}L_2X_4]^{y+}$, as well as mononuclear (N',N^1)$_2$ complexes, $[M^{II}L_2X_2]^{y+}$, where M^{II} is Fe^{II}, Co^{II}, Ni^{II}, Cu^{II} or Zn^{II} (of all of these complexes only some of the Fe(II) complexes are SCO active, hence the choice of Fe(II) in the present work) and X is an anion or solvent molecule (Figure 2).[4,8−10] Clearly other structural types should also be accessible, including $[M^{II}L_3]^{2+}$ species (Figure 2).

The main reason we targeted the **Rdpt** ligands was the potential of their iron(II) complexes to exhibit SCO. Prior to our work there were only two structurally characterized $[ML_3]^{2+}$ complexes in which L contains a triazole-pyridyl

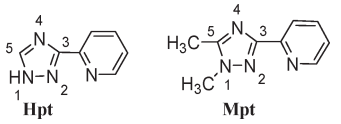

Figure 3. Only pyridyl-triazole containing ligands used prior to this work to generate $[Fe(L)_3]^{2+}$ complexes; both are *mono*-pyridyl-triazoles.

moiety, $[Fe^{II}(Hpt)_3]^{2+}$ and $[Fe^{II}(Mpt)_3]^{2+}$.[11,12] These ligands, **Hpt** and **Mpt** (Figure 3), are *mono*-pyridyl-triazoles, specifically 3-(2-pyridyl)-1,2,4-triazoles where the 1- and 5- substituents are either H or Me, respectively. Both complexes were HS at room temperature but upon cooling underwent a gradual a spin transition. The **Rdpt** ligands are also attractive because of the presence of the π-deficient triazole and pyridine rings which may well facilitate packing interactions in the solid state.

Here we report the preparation and characterization of eight mononuclear tris, $[Fe^{II}L_3]^{2+}$, complexes of a family of di-pyridyl-triazoles, **Rdpt**, in which the only variation is the nature of the N^4 substituent of the triazole ring. The possibility that the electronic properties of the **Rdpt** ligands, and hence the magnetic properties of the iron(II) complexes, may be manipulated by choice of the N^4 substituent is probed, and the structural consequences of this variation are presented.

Results and Discussion

Ligand Selection and Synthesis. The 3,5-dipyridyl triazole based ligands chosen for this study (Figure 1) differ only in the nature of the N^4 substituent, and were all prepared according to our published, general, procedure.[7] Experimental details are provided herein for the new ligand, **Cldpt**, and for **phdpt**, which has been reported previously[13] but has now been made according to our general method.[7]

This series of **Rdpt** ligands contains examples of substituents attached to the triazole nitrogen atom, N^4, via either a carbon (**ibdpt**, **medpt**, **phdpt**, **ptdpt**, **Cldpt**, **pydpt**) or a nitrogen atom (**adpt**, **pldpt**). The amino and alkyl substituted ligands (**adpt, ibdpt** and **medpt**) were selected for their electron donating abilities. The amino group of **adpt** is readily converted to a pyrrolyl group, forming **pldpt**.[10,14] The **pldpt** ligand was chosen as previous crystal structures with other transition metal ions [Co(II), Zn(II), Ni(II), and Cu(II)] showed that the pyrrolyl ring is consistently almost at right angles to the triazole ring, such that minimal π-electron donation occurs. In addition, we were interested in the possibility of enhancing intermolecular interactions by using aromatic substituents off N^4. Hence, the phenyl substituted ligands (**phdpt**), *para*-tolyl (**ptdpt**) and 3,5-dichlorophenyl (**Cldpt**) were studied, along with the 4-pyridyl substituted ligand (**pydpt**) as all of these may facilitate intermolecular $\pi\cdots\pi$ stacking interactions. The electron-withdrawing chloride groups in **Cldpt** may also facilitate intermolecular hydrogen bonding, and the 4-pyridyl group in **pydpt** offers the additional possibility of intermolecular interactions

(8) Kitchen, J. A.; Noble, A.; Brandt, C. D.; Moubaraki, B.; Murray, K. S.; Brooker, S. *Inorg. Chem.* **2008**, *47*, 9450–9458.
(9) (a) Klingele, M. H.; Noble, A.; Boyd, P. D. W.; Brooker, S. *Polyhedron* **2007**, *26*, 479–485. (b) Klingele, M. H.; Boyd, P. D. W.; Moubaraki, B.; Murray, K. S.; Brooker, S. *Eur. J. Inorg. Chem.* **2005**, 910–918. (c) Klingele, M. H.; Brooker, S. *Coord. Chem. Rev.* **2003**, *241*, 119–132.
(10) Klingele, M. H.; Boyd, P. D. W.; Moubaraki, B.; Murray, K. S.; Brooker, S. *Eur. J. Inorg. Chem.* **2006**, 573–589.
(11) Stassen, A. F.; de Vos, M.; van Koningsbruggen, P. J.; Renz, F.; Ensling, J.; Kooijman, H.; Spek, A. L.; Haasnoot, J. G.; Gütlich, P.; Reedijk, J. *Eur. J. Inorg. Chem.* **2000**, 2231.
(12) Sugiyarto, K. H.; Craig, D. C.; Rae, A. D.; Goodwin, H. A. *Aust. J. Chem.* **1995**, *48*, 35–54.
(13) (a) Klingsberg, E. *J. Org. Chem.* **1958**, *23*, 1086–1087. (b) Zhu, D.-R.; Xu, Y.; Zhang, Y.; Wang, T.-W.; You, X.-Z. *Acta Crystallogr., Sect. C* **2000**, *C56*(7), 895–896.
(14) Mandal, S. K.; Clase, H. J.; Bridson, J. N.; Ray, S. *Inorg. Chim. Acta* **1993**, *209*, 1–4.

Table 1. Selected Bond Lengths and Angles for the Seven Structurally Characterized Complexes

bond lengths [Å] and angles [deg]	$[Fe(adpt)_3]^{2+}$	$[Fe(ibdpt)_3]^{2+}$	$[Fe(pldpt)_3]^{2+}$	$[Fe(ptdpt)_3]^{2+}$	$[Fe(pydpt)_3]^{2+}$	$[Fe(phdpt)_3]^{2+}$	$[Fe(Cldpt)_3]^{2+}$
Fe(1)−N(2)[a]	1.950(5)	1.916(2)	1.925(4)	1.933(4)	1.920(2)	1.921(4)	1.939(3)
Fe(1)−N(22)[a]	1.908(4)	1.917(3)	1.954(4)	1.915(4)	1.923(2)	1.911(4)	1.933(3)
Fe(1)−N(42)[a]	1.943(5)	1.923(2)	1.937(4)	1.926(4)	1.940(2)	1.923(4)	1.915(3)
Fe(1)−N(1)[b]	1.965(5)	1.981(2)	1.996(4)	1.990(4)	1.984(2)	1.988(3)	1.992(3)
Fe(1)−N(21)[b]	1.975(5)	1.977(2)	1.995(4)	1.999(4)	1.982(2)	1.974(4)	1.989(3)
Fe(1)−N(41)[b]	1.992(5)	1.986(2)	1.996(4)	1.972(4)	1.989(2)	1.981(4)	1.987(3)
cis-angle range	81.01−100.30	79.73−97.92	80.54−96.72	80.28−96.37	80.37−97.96	80.0−97.7	79.9−100.1
trans-angle range	167.41−174.4	168.66−175.07	170.52−173.23	166.32−174.13	167.97−175.01	167.3−175.3	168.9−176.6

[a] N(2), N(22), and N(42) are triazole nitrogen atoms. [b] N(1), N(21), and N(41) are pyridine nitrogen atoms.

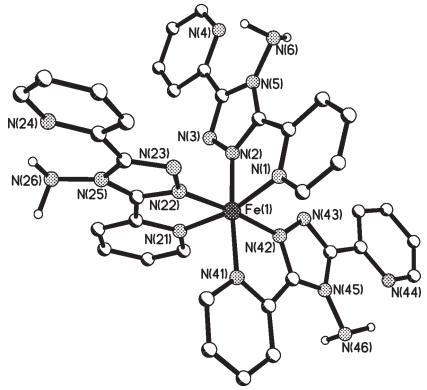

Figure 4. Perspective view of the cation of $[Fe(\mathbf{adpt})_3](BF_4)_2 \cdot 0.5Et_2O$ (hydrogen atoms omitted for clarity).

mediated by either hydrogen bonding or subsequent binding of an additional metal ion.

Synthesis of Complexes. The reaction of the potentially bis-bidentate ligands, **ibdpt**, **medpt**, **adpt, pldpt**,**phdpt**, **ptdpt, Cldpt** and **pydpt** (Figure 1) with $Fe(BF_4)_2 \cdot 6H_2O$ in a 3:1 molar ratio in acetonitrile yielded deep red solid products upon vapor diffusion of diethylether into the red reaction solutions. Microanalytical data were consistent with formulation as $[Fe^{II}(\mathbf{Rdpt})_3](BF_4)_2 \cdot xH_2O$. Infrared data indicated that the ligands were bound asymmetrically to the iron(II) centers as the peaks in the region associated with pyridyl stretching were seen to be split, consistent with coordinated and uncoordinated pyridyl groups. Mass spectral data were also consistent with the formation of the mononuclear tris complexes.

Description of the Structures. Thin orange-red rods of $[Fe(\mathbf{adpt})_3](BF_4)_2 \cdot 0.5Et_2O$ were obtained directly from the MeCN reaction solution by the diffusion of diethyl ether while thin red plates of $[Fe(\mathbf{pldpt})_3](BF_4)_2 \cdot 3MeOH$ were obtained by subsequent recrystallization of the initially obtained solid from hot methanol. Diethyl ether diffusion directly into the MeCN reaction solutions gave single crystals of $[Fe(\mathbf{ibdpt})_3](BF_4)_2 \cdot MeCN$ (red blocks), $[Fe(\mathbf{phdpt})_3](BF_4)_2 \cdot 2MeCN$ (red rods), $[Fe(\mathbf{ptdpt})_3](BF_4)_2 \cdot 1.5MeCN \cdot 0.5H_2O$ (thin red plates), $[Fe(\mathbf{Cldpt})_3](BF_4)_2 \cdot MeCN \cdot Et_2O$ (red blocks), and $[Fe(\mathbf{pydpt})_3](BF_4)_2 \cdot 3.6MeCN \cdot Et_2O$ (red blocks).

The low temperature single crystal structure determinations (Figures 4 and Supporting Information, Figures S1−S6, Table 1) showed the seven complexes to be iso-structural but not isomorphous (Experimental Section). In each case the asymmetric unit contained an iron(II) center coordinated to three bidentate ligands with a distorted octahedral, N_6 coordination sphere. Each potentially bis-bidentate ligand coordinates to the single iron(II) center via only one of its two possible binding pockets. This asymmetric binding mode leads to the possibility of either a *facial* or a *meridional* arrangement of chemically equivalent nitrogen atoms being adopted (Figure 2). All seven complexes crystallized with a *meridional* arrangement (Figure 4 and Supporting Information, Figures S1−S6), as was observed for the related complexes $[Fe(\mathbf{Hpt})_3](BF_4)_2$ and $[Fe(\mathbf{Mpt})_3](BF_4)_2$.[11] Optical isomers of these complexes also exist (Λ and Δ); however, all but one of the seven complexes crystallize as racemates, in centrosymmetric space groups. The exception is $[Fe(\mathbf{phdpt})_3](BF_4)_2.2MeCN$ which crystallizes in the chiral space group $P2_1$ and adopts a right handed helix, the Δ isomer. The bulk sample is expected to comprise equal amounts of crystals in each hand, Λ and Δ.

In each of these low temperature structures the Fe−N bond lengths and *cis*−N−Fe−N bond angles (Table 1) are consistent with those expected for low spin iron(II), being less than 2 Å and close to 90°, respectively. In all cases the $Fe-N_{pyridine}$ bond lengths (1.965−1.998 Å) are longer than the $Fe-N_{triazole}$ bond lengths (1.908−1.954 Å). These observations are consistent with the structural data obtained on $[Fe(\mathbf{Hpt})_3](BF_4)_2$ and $[Fe(\mathbf{Mpt})_3](BF_4)_2$.[11,12]

The **Rdpt** ligands adopt a relatively planar conformation as shown by the relatively small dihedral angles between the mean planes each of the three rings (Supporting Information, Table S1). The constraint imposed by complexation leads to the coordinated pyridine being closer to in plane with the triazole ring (1.2−14.7°, av. = 5.4°) than is the uncoordinated pyridine (2.7−87.0°, av. = 25.9°). The uncoordinated pyridine rings adopt an *anti* configuration with respect to the triazole rings because of repulsion between the nitrogen lone pairs disfavoring the *syn* configuration. The only exception to this is in $[Fe(\mathbf{pldpt})_3](BF_4)_2 \cdot 3MeOH$ where a hydrogen bond from a methanol of solvation to the uncoordinated nitrogen atom N(4) constrains the ligand in this, usually disfavored, *syn* arrangement [O(60)···N(4) = 2.940(6) Å and < (O(60)−H(60)···N(4)) = 142°].

An important feature of the complexes of the **Rdpt** ligands with an aromatic substituent off N^4 (**pldpt**, **phdpt**, **ptdpt**, **Cldpt**, and **pydpt**, Figure 1) is the angle between the aromatic ring and the triazole ring as for efficient π-electron donation/withdrawal the aromatic ring should coplanar with the triazole ring. For $[Fe(\mathbf{pldpt})_3](BF_4)_2$ the pyrrolyl N^4-substituents in the three ligands are almost at right angles to their respective triazole rings [79.4(2)°, 80.4(2)°, and 86.8(2)° for the N(6), N(26), and N(46) rings, respectively] so there will be almost no π-electron donation into the triazole ring. Likewise, the tolyl rings in

[Fe(**ptdpt**)$_3$](BF$_4$)$_2$ [89.8(2)°, 68.0(1)°, and 87.0(1)°], the phenyl rings in [Fe(**phdpt**)$_3$](BF$_4$)$_2$ [76.3(1)°, 86.3(1)°, 79.0 (2)°], and the dichloro-phenyl rings in [Fe(**Cldpt**)$_3$](BF$_4$)$_2$ [70.3(1)°, 78.4(1)°, and 73.0(5)/ 75.2(5)° (the third N^4-substituent contains a disorder over two sites, so an extra angle is included)] are almost at right angles to the attached triazole rings. The angles formed between the 4-pyridyl groups and the attached triazole rings in [Fe(**pydpt**)$_3$](BF$_4$)$_2$, while still large, are not as close to 90° [66.9(1)°, 63.5(1)°, and 77.4(1)°].

Packing Analysis. Our recent systematic investigation of the analogous nickel(II) tris-**Rdpt** complexes revealed the presence of many anion-π and acetonitrile-π interactions,[15] the first time such interactions[16,17] had been noted for a triazole ring. That study identified the presence of anions in "π-pockets" (formed by two coordinated triazole rings and one coordinated pyridine ring) and forming "π-sandwiches" (in which the triazole ring is "sandwiched" by two anions), as well as the more typical types of anion-π interactions. The triazole rings thus facilitated extended interactions through the lattice, something that can be critically important in iron(II) SCO systems (see Introduction).

The π-pocket in the present complexes occurs as a result of them adopting the *mer* configuration and, unlike the nickel(II) analogues (which are also *mer*),[15] involves two triazole rings within the same complex, rather than one triazole and one pyridyl ring.

With the bulky nature of the cations in this family of [Fe^{II}(**Rdpt**)$_3$](BF$_4$)$_2$·*xsolvent* complexes it is understandable that the packing is complex with no well-defined sheets or planes. However, as for the Ni(II) analogues,[15] there are many interesting short contacts that link the cationic complexes to tetrafluoroborate anions and solvent molecules (Figures 5−7, Supporting Information, Figures S7−S21). In each of the iron(II) complexes there are at least nine aromatic rings (three ligands each with two 2-pyridyl rings and a triazole ring), giving rise to many π-based interactions. Combinations of $\pi\cdots\pi$, (offset and edge-to-face), anion$\cdots\pi$, C−H$\cdots\pi$, and acetonitrile$\cdots\pi$ interactions are observed. These complexes also display a large number of hydrogen bonding interactions (O−H or N−H donors). One complex, [Fe(**Cldpt**)$_3$](BF$_4$)$_2$, also displays halogen$\cdots$halogen interactions.[18] Details of these interactions are provided in the Supporting Information; however, three of the most interesting examples are described here. In [Fe(**pydpt**)$_3$](BF$_4$)$_2$·3.6MeCN·Et$_2$O, a triazole ring is sandwiched by two acetonitrile solvent molecules (Figure 5). The acetonitrile molecules adopt differing arrangements such that N(80) points at the triazole centroid and is perpendicular to the triazole mean plane, while N(60) is parallel to the plane. The interaction between N(80) and the triazole

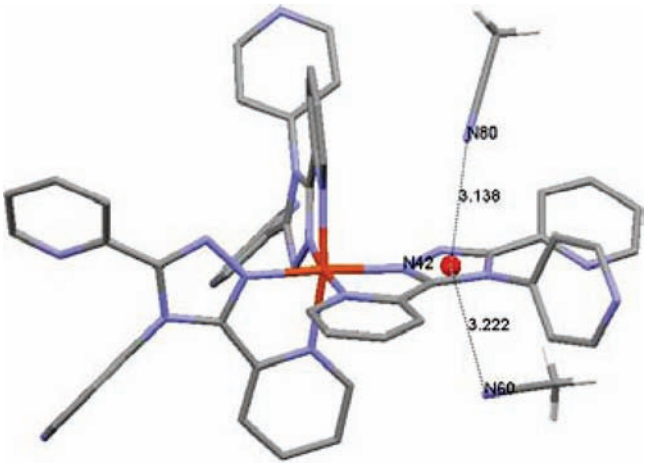

Figure 5. Perspective view of the acetonitrile "π-sandwich" present in the structure of [Fe(**pydpt**)$_3$](BF$_4$)$_2$·3.6MeCN·Et$_2$O (hydrogen atoms omitted for clarity).

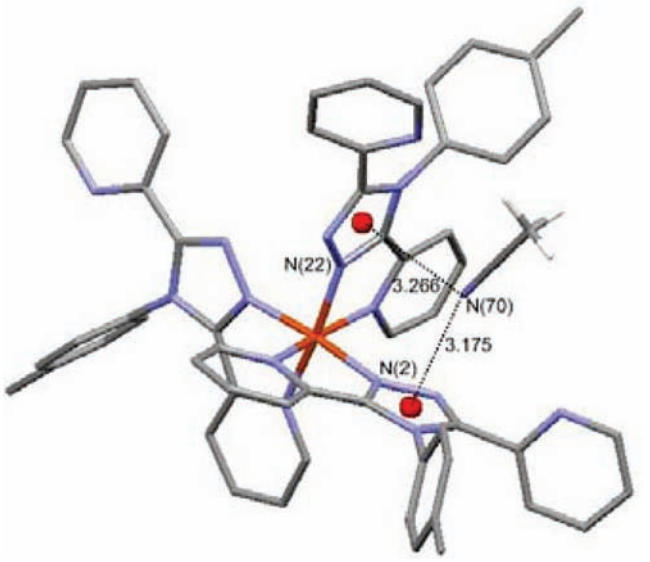

Figure 6. Perspective view of the acetonitrile-π interations within the triazole "π-pocket" present in the structure of [Fe(**ptdpt**)$_3$](BF$_4$)$_2$·1.5 MeCN (hydrogen atoms omitted for clarity).

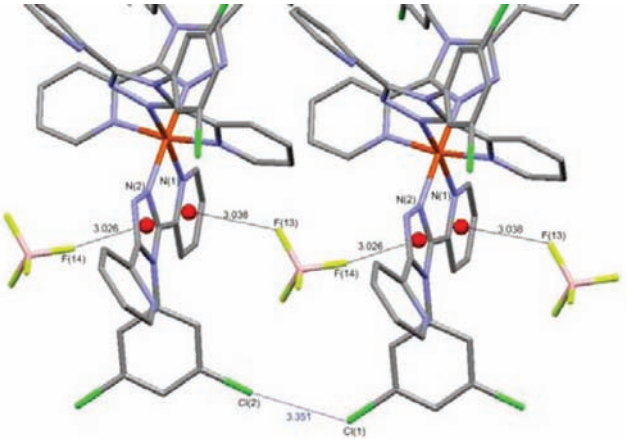

Figure 7. Perspective view of the repeating (anion-π-anion-π)$_\infty$ interactions, and of the Cl$\cdots$Cl interactions, present in the structure of [Fe(**Cldpt**)$_3$](BF$_4$)$_2$·MeCN·Et$_2$O (hydrogen atoms omitted for clarity).

(15) White, N. G.; Kitchen, J. A.; Brooker, S. *Eur. J. Inorg. Chem.* **2009**, 1172–1180.
(16) Mooibroek, T. J.; Teat, S. J.; Massera, C.; Gamez, P.; Reedijk, J. *Cryst. Growth Des.* **2006**, *6*(7), 1569–1574.
(17) (a) Gamez, P.; Mooibroek, T. J.; Teat, S. J.; Reedijk, J. *Acc. Chem. Res.* **2007**, *40*, 435–444. (b) Mooibroek, T. J.; Black, C. A.; Gamez, P.; Reedijk, J. *Cryst. Growth Des.* **2008**, *8*(4), 1082–1093.
(18) (a) Espallargas, G. M.; Brammer, L.; Allan, D. R.; Pulham, C. R.; Robertson, N.; Warren, J. E. *J. Am. Chem. Soc.* **2008**, *130*, 9058–9071. (b) Zordan, F.; Brammer, L.; Sherwood, P. *J. Am. Chem. Soc.* **2005**, *127*, 5979–5989.

centroid (3.138 Å) is stronger than the parallel acetonitrile interaction to the triazole centroid (3.222 Å), consistent with the findings of Reedijk and co-workers with other heterocycles.[16] In [Fe(**ptdpt**)$_3$](BF$_4$)$_2$·1.5MeCN (Figure 6) acetonitrile-π interactions occur in which an acetonitrile molecule interacts with both of the π-pocket triazole rings. This interaction once again results in one perpendicular and one parallel interaction, with respect to the triazole mean plane. Again the perpendicular interaction is stronger (3.175 Å) than the parallel interaction (3.266 Å). In the final example (Figure 7) a repeating anion-π-anion-$\pi\cdots$ interaction is observed in [Fe(**Cldpt**)$_3$](BF$_4$)$_2$·MeCN·Et$_2$O. The anion-π interactions involve the highly π acidic triazole ring, as well as a coordinated pyridine ring. Alongside this is a chlorine-chlorine interaction. These structures (Figures 5−7 and Supporting Information, Figures S7−S21) confirm that the nature of the N^4-substituent does influence the packing interactions in the resulting complexes (also evident from C−H$\cdots\pi$ interactions in [Fe(**ptdpt**)$_3$](BF$_4$)$_2$·1.5 MeCN, Supporting Information, Figure S16).

Magnetochemistry. Magnetic measurements were carried out from 350 to 4.2 K on solid samples of all eight complexes. [Fe(**adpt**)$_3$](BF$_4$)$_2$·2$^1/_2$H$_2$O, [Fe(**ibdpt**)$_3$](BF$_4$)$_2$·H$_2$O, [Fe(**ptdpt**)$_3$](BF$_4$)$_2$·2$^1/_2$H$_2$O, [Fe(**pydpt**)$_3$](BF$_4$)$_2$·1$^1/_2$H$_2$O, [Fe(**phdpt**)$_3$](BF$_4$)$_2$·1$^1/_2$H$_2$O, [Fe(**Cldpt**)$_3$](BF$_4$)$_2$, and [Fe(**medpt**)$_3$](BF$_4$)$_2$·1$^1/_2$H$_2$O were low spin at all temperatures studied. In contrast, while [Fe(**pldpt**)$_3$](BF$_4$)$_2$·1$^1/_2$H$_2$O is in the low spin state (μ_{eff} = 0.86 μ_B) from 4.2 K up to about 300 K, a gradual spin transition begins to occur above this temperature (Figure 8). Subsequently this complex was studied from 150 to 400 K (Figure 8, inset), but even at 400 K the transition is incomplete. An attempt to carry out variable temperature X-ray analysis on a single crystal of [Fe(**pldpt**)$_3$](BF$_4$)$_2$·3MeOH showed that at temperatures above 350 K the crystal loses crystallinity, and that before this there is minimal change in the unit cell dimensions (expect an increase in these when changing from LS to HS).[19]

Variable Temperature NMR. The diamagnetic low-spin iron(II) center present in all of these [Fe(**Rdpt**)$_3$](BF$_4$)$_2$ complexes in the solid state at room temperature, led to the expectation that solution studies using NMR spectroscopy, in deuterated nitromethane, would be informative.

As expected, compared to the signals seen for the respective free ligand there are clear shifts on complexation. In all cases the asymmetric binding mode of the **Rdpt** ligand seen in the solid state was clearly retained in solution as signals for both the coordinated and uncoordinated pyridine rings of the **Rdpt** ligand were observed.

Variable temperature (VT) NMR studies, on all eight [Fe(**Rdpt**)$_3$](BF$_4$)$_2$ complexes, showed that as the temperature was increased (a) the asymmetric binding mode is retained and (b) the coordinated pyridine ring protons shift downfield and broaden to some extent (Figures 9, Supporting Information, Figures S23−S30). The [Fe^{II}(**pldpt**)$_3$](BF$_4$)$_2$ complex showed the largest shifts so is discussed here (Figure 9): the biggest shift seen for any signal in any complex is found in this complex, and

(19) Kitchen, J. A.; Halder, G. J.; Kepert, C. J.; Brooker, S., unpublished results.

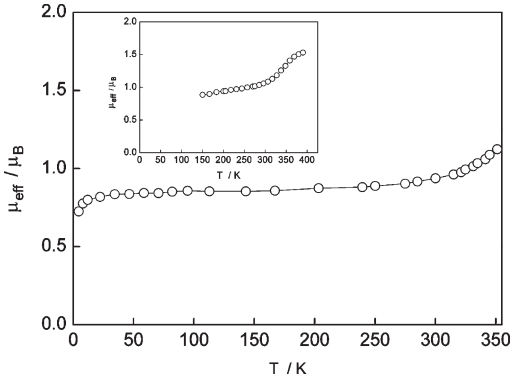

Figure 8. Plot of μ_{eff} (BM) vs temperature (K) for [Fe(**pldpt**)$_3$](BF$_4$)$_2$·1$^1/_2$H$_2$O. Circles are data points; solid line simply joins the data points.

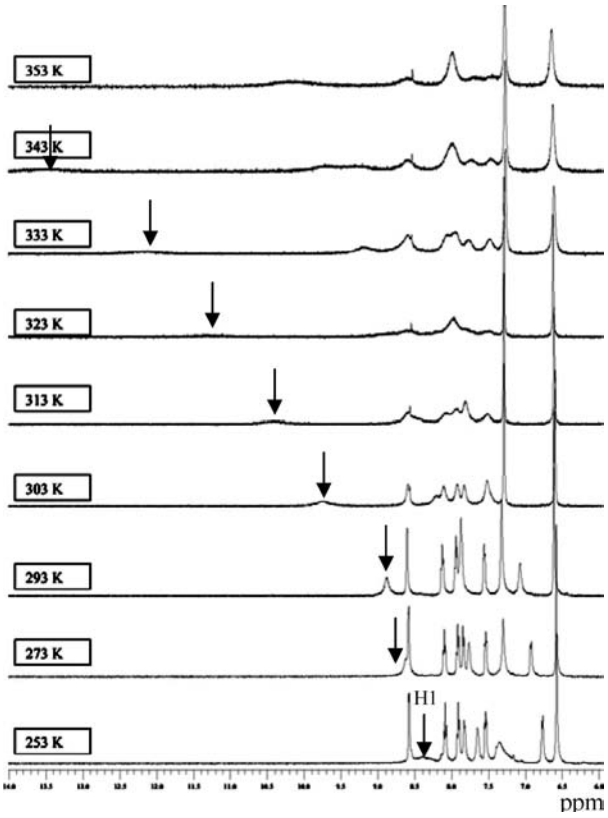

Figure 9. ^{1}H NMR spectra vs temperature (K) for [Fe(**pldpt**)$_3$](BF$_4$)$_2$·1$^1/_2$H$_2$O in deuterated nitromethane The coordinated pyridyl proton (H1, Figure 1) is marked.

involves the signal for the coordinated pyridyl ring proton 1 (Figure 1) moving from ~8.5 ppm at −20 °C to ~15 ppm at 80 °C. A VT NMR experiment carried out on the free ligand, **pldpt** (Supporting Information, Figures S31), showed no large downfield shift of any of the proton signals. Therefore the downfield shift seen for the complex is believed to be due to the formation of a paramagnetic species. In previous work it was observed that the diamagnetic [Fe(**Rdpt**)$_3$](BF$_4$)$_2$ complex and the paramagnetic complexes [Fe$_2$(**Rdpt**)$_2$X$_4$](BF$_4$)$_4$ or [Fe(**Rdpt**)$_2$X$_2$](BF$_4$)$_n$ can be obtained from the same reaction solution.[8] Therefore it appears that on dissolution of these [Fe(**Rdpt**)$_3$](BF$_4$)$_2$ complexes, equilibria are established that lead to the formation of traces of such paramagnetic complexes at elevated temperatures,

leading to the observed VT NMR behavior (e.g., Figure 9).

To test this proposed explanation, an iron(II) complex of the unsymmetrical ligand 4-toluene-3-(2-pyridyl)-5-phenyl-4*H*-1,2,4-triazole (**ptmpt**),[7] $[Fe(\mathbf{ptmpt})_3](BF_4)_2$, was prepared. As this ligand has only one of the two five-membered chelate pockets that the **Rdpt** ligands have, its use should prevent the formation of a paramagnetic dinuclear complex, although a paramagnetic mononuclear complex, $[Fe(\mathbf{ptmpt})_2X_2](BF_4)_n$ could still be formed. Once again a downfield shift was observed on heating from 30 to 70 °C (Supporting Information, Figures S27). In this case the shift is most likely due to the formation of a paramagnetic mononuclear complex with *trans* axial water molecules, $[Fe(\mathbf{Rdpt})_2(H_2O)_2](BF_4)_2$. A complex of this type, $[Fe^{II}(\mathbf{Cldpt})_2(H_2O)_2](CF_3SO_3)_2$, has been isolated and is HS.[20] Such a species is a better candidate for the proposed trace amount of paramagnetic species in solution at elevated temperatures as it has a more likely stoichiometry, retains an asymmetric ligand binding mode, and is a sterically undemanding structural type.

^{15}N NMR and Density Functional Theory (DFT) Calculations. The effect that the choice of N^4-substituent has on the chemical shift of the nitrogen atoms, in particular the triazole N^1 and N^2 nitrogen atoms, was examined by ^{15}N NMR spectroscopy. This study was undertaken as an initial attempt to gain some understanding of what effect the N^4-substituent is having on the coordinating nitrogen atoms. This might allow one to establish trends between experimentally determined and calculated spectra such that we could predict what ligands would give SCO without the current trial and error approach.

The metal-free **Rdpt** ligands have been analyzed as they are very soluble, so the ^{15}N NMR spectra can be obtained in a timely fashion (Figure 10, Table 2). Spectra were recorded either by direct monitoring of the ^{15}N nucleus or by HMBC methods through coupling to nearby protons. There is clearly a variation in the chemical shift of these nitrogen atoms on changing the N^4-substituent (Table 2). Ring based N^4 substituents seem to impart a higher chemical shift on N^{pyr} (309.6−312.5 ppm) than the more electron donating alkyl and amino substituents do (295.1−306.4 ppm). Interestingly, the signal for N^1 is similar for all ligands (316.1−318.3 ppm) except for those with nitrogen based, amino, and pyrrolyl substituents for which it is at a lower chemical shift (310.9−311.9 ppm). Strangely, the highest chemical shifts for N^1 are seen for the methyl and iso-butyl ligands (317.6, 318.3 ppm), while all ligands with phenyl or pyridyl based N^4-substituents have lower, nearly identical chemical shifts (316.1−316.9 ppm). All of the N^4 chemical shifts occur at far lower values (156.5−183.3 ppm) than those observed for N^{pyr} and N^1 (295.1−318.3 ppm), and as expected it varies the most significantly as the N^4-substituent is changed (156.5−183.3 ppm). The remainder of the substituents fall in a more compact range (168.9−176.6 ppm).

Calculations of the expected ^{15}N chemical shifts of these **Rdpt** ligands using DFT methods were carried out.[21] Density functional calculations of the ^{15}N chemical shifts [B3LYP/6-311G(d,p)//B3LYP/6-311 + G(2d,p)] are in reasonable agreement with the measured values (Table 2). Differences have been ascribed to an overestimation of the negative paramagnetic contribution to the shieldings.[22] The lowest shift for N^4 occurs for the methyl substituent (156.5 ppm), and the highest for the amino substituent (183.3 ppm). We had expected similar

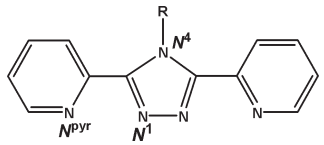

Figure 10. Diagram of numbering scheme used for ^{15}N NMR experiments and modeling of the **Rdpt** ligands (see Table 2).

Table 2. Comparison of Experimentally Determined and Calculated (in Brackets) ^{15}N NMR Signals for the Family of Metal-Free **Rdpt** Ligands[a]

R group	N^{pyr}(calcd)	N^1(calcd)	N^4(calcd)
amino	295.1 (291.2)	310.9[b] (335.3)	183.3[b] (189.4)
pyrrol	309.6 (312.7)	311.9[b] (329.5)	176.6 (176.0)
methyl	306.4 (303.4)	317.6[b] (360.1)	156.5 (157.3)
iso-butyl	306.3 (303.9)	318.3[b] (340.6)	168.9 (169.6)
4-pyridyl	312.3 (311.9)	316.9[b] (335.4)	173.0 (170.4)
3,5-dichlorophenyl	311.3 (311.4)	316.5[b] (335.4)	171.5 (169.2)
4-methylphenyl	312.5 (312.9)	316.6[b] (335.9)	175.6 (172.7)
phenyl	312.3 (312.8)	316.1[b] (335.3)	175.9 (173.3)

[a] See Figure 1 for these ligands, and Figure 10 for the nitrogen atom numbering scheme employed. [b] Direct (^{15}N NMR) measurement [DCM solutions in 10 mm tubes with separate 5 mm tube of CD_3NO_2 inserted as a reference (4.33 ppm)]; all other measurements by indirect (HMBC) measurement in $CDCl_3$ referenced to nitromethane.

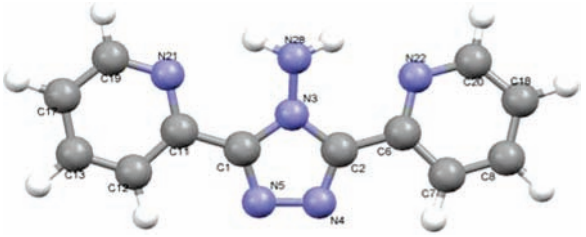

Figure 11. Calculated structure of 4-amino-3,5-di(2-pyridyl)-1,2,4-triazole, **adpt**, B3LYP/6-311G(d,p).[21] Selected metric details (Å) from the calculation with experimental values from ref 24 in parentheses: N3−N28 1.404 (1.410), N3−C2 1.368 (1.360), C2−N4 1.330 (1.319), N4−N5 1.345 (1.367), C2−C6 1.462 (1.469), H−N22 2.093 (2.078, 2.388).

(20) Kitchen, J. A.; Brooker, S., unpublished results.

(21) Frisch, M. J. G. W. T. S., H. B.; Scuseria, G. E.; Robb, M. A.; Cheeseman, J. R.; Montgomery, Jr., J. A.; Vreven, T.; Kudin, K. N.; Burant, J. C.; Millam, J. M.; Iyengar, S. S.; Tomasi, J.; Barone, V.; Mennucci, B.; Cossi, M.; Scalmani, G.; Rega, N.; Petersson, G. A.; H. N.; Hada, M.; Ehara, M.; Toyota, K.; Fukuda, R.; Hasegawa, J.; Ishida, M.; Nakajima, T.; Honda, Y.; Kitao, O.; Nakai, H.; Klene, M.; Li, X.; Knox, J. E.; Hratchian, H. P.; Cross, J. B.; Adamo, C.; Jaramillo, J.; Gomperts, R.; Stratmann, R. E.; Yazyev, O.; Austin, A. J.; Cammi, R.; Pomelli, C.; Ochterski, J. W.; Ayala, P. Y.; Morokuma, K.; Voth, G. A.; Salvador, P.; Dannenberg, J. J.; Zakrzewski, V. G.; Dapprich, S.; Daniels, A. D.; Strain, M. C.; Farkas, O.; Malick, D. K.; Rabuck, A. D.; Raghavachari, K.; Foresman, J. B.; Ortiz, J. V.; Cui, Q.; Baboul, A. G.; Clifford, S.; Cioslowski, J.; Stefanov, B. B.; Liu, G.; Liashenko, A.; Piskorz, P.; Komaromi, I.; Martin, R. L.; Fox, D. J.; Keith, T.; Al-Laham, M. A.; Peng, C. Y.; Nanayakkara, A.; Challacombe, M.; Gill, P. M. W.; Johnson, B.; W. C.; Wong, M. W.; Gonzalez, C.; Pople, J. A. *Gaussian 03*, Gaussian, Inc.: Wallingford, CT, 2003.

(22) Bühl, M.; Kaupp, M.; Malkina, O. L.; Malkin, L. *J. Comput. Chem.* **1999**, *20*, 91.

values for these two as they are both strong electron donating substituents. The charges at atoms N^4 and N^1 were calculated for the amino and methyl derivatives, using the NBO method[23] (for N^4 and N^1 respectively: amino −0.17 and −0.29; methyl −0.36 and −0.30). The variation in charges at N^4 can be attributed to the relative polarities of the N−N and C−N σ bonds. The change in chemical shift of the N^4 nuclei is due almost entirely to the differing paramagnetic contributions (27.7 ppm). The amino substituent has the ability to hydrogen bond to the pyridine nitrogen atoms (Figure 11), and this may also influence the observed chemical shift. A calculation of the N^4 chemical shift for the ligand conformation found in the X-ray crystal structure of $[Fe(\mathbf{adpt})_3](BF_4)_2\cdot 0.5Et_2O$,[24] which has only one hydrogen bond to a pyridine group, shows a shift of 14.2 ppm to 175.2 ppm and a charge of −0.21.

Conclusion

Reactions employing a 1:3 metal to ligand ratio of iron(II) tetrafluoroborate hexahydrate to **adpt**, **pldpt**, **pydpt**, **phdpt**, **ptdpt**, **Cldpt**, **medpt**, **ibdpt**, and **ptmpt**, in acetonitrile, gave the desired family of hydrated products $[Fe^{II}(\mathbf{Rdpt})_3](BF_4)_2\cdot xH_2O$. All nine of the complexes appear to be LS at all temperatures, with the exception of $[Fe^{II}(\mathbf{pldpt})_3](BF_4)_2\cdot 1^1/_2H_2O$ which shows the beginnings of SCO at higher temperatures. In d_3-nitromethane solution these mononuclear tris complexes appear to be somewhat unstable as the signals in the ^{1}H NMR spectra become broad and shift downfield as the temperature increases, implying the formation of a HS species.

The seven structurally characterized complexes all crystallized as *mer* isomers, the constraint of which resulted in two triazole rings forming a "π-pocket", capable of interacting with anions or solvent molecules. A careful packing analysis as a function of N^4-substituent revealed many short contacts, including classical and non-classical (C−H donors) hydrogen bonding, $\pi\cdots\pi$ stacking, C−H$\cdots\pi$, anion$\cdots\pi$, solvent$\cdots\pi$, and halogen$\cdots$halogen interactions. The extent and nature of these depended on the **Rdpt** N^4-substituent. The majority of complexes displayed interactions between tetrafluoroborate anions or acetonitrile molecules and the π-pocket; the exception was $[Fe(\mathbf{ibdpt})_3](BF_4)_2$ where the bulky isobutyl substituent blocked the π-pocket preventing such interactions. Complexes where the N^4-substituent was directly involved in intermolecular interactions involved the ligands **adpt**, **ptdpt**, and **Cldpt**, and these contained N−H hydrogen bonding, C−H$\cdots\pi$ interactions, and Cl$\cdots$Cl interactions, respectively. Therefore, for efficient intermolecular interactions involving the N^4-substituent it seems that additional functionality is required.

DFT calculations of ^{15}N NMR chemical shifts for these **Rdpt** ligands are in good agreement with the experimentally obtained values. Combining the trends observed here, that is, between experimentally determined and calculated ^{15}N chemical shifts, and the trends we are developing through the preparation and characterization of families of iron(II) **Rdpt** complexes, in particular how the N^4-substituent influences the magnetic properties, might in the future allow us to predict which ligands will most likely give SCO in iron(II) and to tune the SCO behavior by varying the N^4-substituent. Using calculations to "test" the suitability of a ligand, by predicting the ^{15}N NMR spectrum and comparing the predicted chemical shifts to those of a ligand known to give an SCO active complex, should allow us to survey many ligands, containing many different N^4-substituents, with relative ease. This would remove the need to synthesize all ligands and complexes of interest and allow us to focus instead just on those that will likely have the desired properties.

While it was disappointing that, other than $[Fe^{II}(\mathbf{pldpt})_3](BF_4)_2\cdot 1^1/_2H_2O$, all complexes were LS from 4 to 300 K, this study is nevertheless an important first step toward screening ligand properties by calculation prior to synthesis. It has also revealed new types of anion-π intermolecular interactions between the mononuclear complexes in the solid state; these interactions may aid in mediating the communication needed for abrupt SCO with hysteresis or indeed act as the perturbation (anion-ligand interactions can alter the ligand field strength[25]) required to induce SCO as observed recently by Shores and co-workers.[26]

Experimental Section

General Remarks. All solvents were laboratory reagent grade except acetonitrile which was HPLC grade and was distilled from calcium hydride before use. $Fe(BF_4)_2\cdot 6H_2O$ was purchased from Aldrich and used as received. The igands, 4-amino-3,5-di-(2-pyridyl)-4*H*-1,2,4-triazole (**adpt**), 4-(1*H*-pyrrol-1-yl)3,5-di-(2-pyridyl-4*H*-1,2,4-triazole (**pldpt**), 4-isobutyl-3,5-di(2-pyridyl)-4*H*-1,2,4-triazole (**ibdpt**), 4-methyl-3,5-di(2-pyridyl)-4*H*-1,2,4-triazole (**medpt**), 4-(4-pyridyl)-3,5-di(2-pyridyl)-4*H*-1,2,4-triazole (**pydpt**), 4-(*para*-tolyl)-3,5-di(2-pyridyl)-4*H*-1,2,4-triazole (**ptdpt**), and 4-(*para*-tolyl)-3-phenyl-5-(2-pyridyl)-4*H*-1,2,4-triazole (**ptmpt**) were prepared as described earlier[7,10,14,27] Elemental analyses were carried out by the Campbell Microanalytical Laboratory at the University of Otago. ^{1}H NMR spectra were recorded with a Varian INOVA-500 spectrometer at 25 °C. The variable temperature studies were typically carried out on 5−10 mg of complex dissolved in (~0.75 mL) d_3-nitromethane, with the spectra obtained at 10−20° intervals over a temperature range of −25 to 80 °C. ^{15}N NMR (direct) were recorded on a Varian INOVA-500 spectrometer by Dr Mervyn Thomas (Otago), while indirect HMBC measurements were recorded by Dr Maruta Boyd (Cancer Research Institute, Auckland) on a Bruker Advance 400 spectrometer. Infrared spectra were recorded over the range 4000−400 cm^{-1} with a Perkin−Elmer Spectrum BX FT-IR spectrophotometer. X-ray data were collected with a Bruker APEX II area detector diffractometer, using graphite-monochromated Mo Kα radiation (λ = 0.71073 Å) at the University of Otago (Table 3). The data were corrected for Lorentz and polarization effects and semiempirical absorption corrections (SCALE) were applied. The structures were solved by direct methods (SHELXS-97) and refined against all F^2 data (SHELXL-97).[28] Hydrogen atoms were inserted at calculated positions and rode on the atoms to which they were attached, and all non-hydrogen atoms were made anisotropic. Magnetic data were recorded at Monash University over the range 300−4.2 K with a Quantum Design MPMS5

(23) Glendening, E. D.; Read, A. E.; Carpenter, J. E.; Weinhold, F. *NBO* (version 3.1); Gaussian, Inc.: Pittsburgh, PA, 2003.
(24) Ramos Silva, M.; Silva, J. A.; Martins, N. D.; Matos Beja, A.; Sobral, A. J. F. N. *Acta Crystallogr., Sect. E* **2008**, *64*, o1762.
(25) (a) Lemercier, G.; Brefuel, N.; Shova, S.; Wolny, J. A.; Dahan, F.; Verelst, M.; Paulsen, H.; Trautwein, A.; Tuchagues, J. P. *Chem.—Eur. J.* **2006**, 7421–7432. (b) Goodwin, H. A. *Top. Curr. Chem.* **2004**, *233*, 59–90.
(26) Ni, Z.; Shores, M. P. *J. Am. Chem. Soc.* **2009**, *131*, 32–33.
(27) Geldard, J. F.; Lions, F. *J. Org. Chem.* **1965**, *30*, 318–319.
(28) Sheldrick, G. M. *Acta Crystallogr., Sect. A* **2008**, *A64*, 112–122.

Table 3. Crystal Structure Determination Details for the Complexes [Fe(**adpt**)$_3$](BF$_4$)$_2$·0.5Et$_2$O, [Fe(**ibdpt**)$_3$](BF$_4$)$_2$·MeCN, [Fe(**pldpt**)$_3$](BF$_4$)$_2$·3MeOH, [Fe(**phdpt**)$_3$](BF$_4$)$_2$·2MeCN, [Fe(**ptdpt**)$_3$](BF$_4$)$_2$·1.5MeCN·0.5H$_2$O, [Fe(**pydpt**)$_3$](BF$_4$)$_2$·3.6MeCN·Et$_2$O, and [Fe(**Cldpt**)$_3$](BF$_4$)$_2$·MeCN·Et$_2$O

	[Fe(adpt)$_3$]-(BF$_4$)$_2$·0.5Et$_2$O	[Fe(ibdpt)$_3$]-(BF$_4$)$_2$·MeCN	[Fe(pldpt)$_3$]-(BF$_4$)$_2$·3MeOH	[Fe(phdpt)$_3$]-(BF$_4$)$_2$·2MeCN	[Fe(ptdpt)$_3$]-(BF$_4$)$_2$·1.5MeCN·0.5H$_2$O	[Fe(pydpt)$_3$]-(BF$_4$)$_2$·3.6MeCN·Et$_2$O	[Fe(Cldpt)$_3$]-(BF$_4$)$_2$·MeCN·Et$_2$O
empirical formula	C38 H35 B2 F8 Fe N18 O0.50	C50 H54 B2 F8 Fe N16	C51 H48 B2 F8 Fe N18 O3	C58 H45 B2 F8 Fe N17	C60 H49.50 B2 F8 Fe N16.50 O0.50	C62.20 H56.80 B2 F8 Fe N21.60 O	C60 H46 B2 Cl6 F8 Fe N16 O
formula weight	981.31	1108.56	1190.54	1209.58	1239.13	1352.36	1449.30
temperature	83(2) K	90(2) K	89(2) K	90(2) K	89(2) K	89(2) K	90(2) K
wavelength	0.71073 Å	0.71073 Å	0.71073 Å	0.71073 Å	0.71073 Å	0.71073 Å	0.71073 Å
crystal system	monoclinic	monoclinic	monoclinic	monoclinic	monoclinic	triclinic	monoclinic
space group	$P2_1/c$	$P2_1/c$	$P2_1/n$	$P2_1$	$C2/c$	$P\bar{1}$	$P2_1/c$
unit cell dimensions							
a, Å	8.4543(4)	17.0823(5)	19.678(2)	8.9268(5)	21.1552(18)	13.4095(11)	29.1742(6)
b, Å	39.1291(19)	15.4084(4)	14.6766(15)	13.0747(8)	20.5932(17)	14.0655(11)	8.5414(2)
c, Å	14.6110(7)	20.5003(6)	21.096(2)	24.2774(14)	26.412(2)	19.2009(15)	26.1751(5)
α, deg	90°	90°	90°	90°	90°	77.367(4)°	90°
β, deg	106.119(2)°	105.1740(10)°	116.573(5)°	95.734(4)°	96.329(5)°	69.590(4)°	103.915(1)°
γ, deg	90°	90°	90°	90°	90°	74.564(4)°	90°
Volume, Å^3	4643.4(4)	5207.8(3)	5449.1(10)	2819.4(3)	11436.3(17)	3239.8(4)	6331.1(2)
Z	4	4	4	2	8	2	4
density (calculated), Mg/m^3	1.404	1.414	1.451	1.425	1.439	1.386	1.521
absorption coefficient, mm^{-1}	0.409	0.372	0.366	0.351	0.348	0.316	0.572
F(000)	2004	2296	2448	1240	5096	1394	2944
crystal size, mm^3	0.70 × 0.04 × 0.04	0.29 × 0.19 × 0.11	0.18 × 0.10 × 0.10	0.39 × 0.10 × 0.02	0.24 × 0.21 × 0.15	0.40 × 0.18 × 0.10	0.24 × 0.20 × 0.03
theta range for data collection	1.04−26.50°	1.91−26.40°	1.76−26.44°	1.77−26.42°	1.38−24.00°	1.77−26.42°	0.72−26.41°
index ranges	$-10 \le h \le 10$ $-48 \le k \le 48$ $-18 \le l \le 18$	$-21 \le h \le 14$ $-19 \le k \le 18$ $-15 \le l \le 25$	$-24 \le h \le 24$ $-18 \le k \le 18$ $-26 \le l \le 26$	$-11 \le h \le 11$ $-16 \le k \le 16$ $-30 \le l \le 30$	$-24 \le h \le 24$ $-23 \le k \le 22$ $-30 \le l \le 30$	$-14 \le h \le 16$ $-17 \le k \le 17$ $-24 \le l \le 23$	$-36 \le h \le 32$ $-10 \le k \le 10$ $-30 \le l \le 32$
reflections collected	108619	27882	89170	30087	55983	54496	60478
independent reflections	9566 [R(int) = 0.1941]	9597 [R(int) = 0.0646]	11169 [R(int) = 0.1912]	11259 [R(int) = 0.0850]	8971 [R(int) = 0.1549]	13000 [R(int) = 0.0453]	12963 [R(int) = 0.0715]
completeness to theta = 26.50°	99.2%	89.8%	99.4%	99.3%	100.0%	97.6%	99.6%
absorption correction	semiempirical from equivalents	semiempirical from equivalents	semiempirical from equivalents	semiempirical from equivalents	semiempirical from equivalents	semiempirical from equivalents	semiempirical from equivalents
max. and min transmission	1.000 and 0.788	0.9603 and 0.8999	1.000 and 0.379302	0.9930 and 0.8754	0.9496 and 0.8121	0.9691 and 0.7914	1.000 and 0.908
refinement method	full-matrix least-squares on F^2	full-matrix least-squares on F^2	full-matrix least-squares on F^2	full-matrix least-squares on F^2	full-matrix least-squares on F^2	full-matrix least-squares on F^2	full-matrix least-squares on F^2
data/restraints/parameters	9566/43/626	9597/33/739	11169/43/817	11259/1/778	8971/0/806	13000/0/910	12963/48/897
goodness-of-fit on F^2	1.033	1.018	1.018	0.980	0.915	1.044	1.031
final R indices [$I > 2$sigma(I)]	R1 = 0.0792, wR2 = 0.2239	R1 = 0.0509, wR2 = 0.1079	R1 = 0.0719, wR2 = 0.1682	R1 = 0.0620, wR2 = 0.1200	R1 = 0.0561, wR2 = 0.1298	R1 = 0.0526, wR2 = 0.1306	R1 = 0.0559, wR2 = 0.1318
R indices (all data)	R1 = 0.1646, wR2 = 0.2705	R1 = 0.0957, wR2 = 0.1275	R1 = 0.1648, wR2 = 0.2193	R1 = 0.1040, wR2 = 0.1375	R1 = 0.1347, wR2 = 0.1562	R1 = 0.0740, wR2 = 0.1429	R1 = 0.0913, wR2 = 0.1489
largest diff. peak and hole	1.283 and −0.609 e Å^{-3}	0.643 and −0.438 e Å^{-3}	0.672 and −0.860 e Å^{-3}	0.432 and −0.523 e Å^{-3}; Flack x parameter = −0.02(2)	0.690 and −0.469 e Å^{-3}	1.333 and −0.460 e Å^{-3}	1.102 and −0.573 e Å^{-3}

SQUID magnetometer with an applied field of 1 T. ESI mass spectra were recorded in acetonitrile using a Bruker MicrOTOF$_Q$ spectrometer by Mr. Ian Stewart (Otago).

***N*-3,5-dichlorophenyl-2-pyridinecarbothioamide.** A mixture of 3,5-dichlorophenylaniline (8.10 g, 50.0 mmol), sulfur (4.81 g, 150 mmol), and sodium sulfide nonahydrate (0.240 g, 1.00 mmol) was refluxed for 48 h in 30 mL of 2-picoline. The resulting dark solid was dried thoroughly in vacuo and recrystallized from 700 mL of boiling 1:1 MeOH/EtOAc. On cooling, fine brown crystals precipitated from the solution. These were collected by filtration, washed with ice-cold MeOH (50 mL), and dried thoroughly in vacuo. Two further crops of crystals were grown by slow evaporation of the mother liquor. These were isolated, washed and dried in the same way. Combined yield: 11.5 g (82%). $C_{12}H_8N_2SCl_2$: calcd C 50.90, H 2.85, N 9.89; found C 50.86, H 2.99, N 9.82%. ^{1}H NMR ($CDCl_3$): δ 12.10 (br s, 1H, N*H*), 8.75 (ddd, $J_{3,4}$ = 8 Hz, $J_{3,5}$ = 1 Hz, $J_{3,6}$ = 1 Hz, 2H, 2 × pyH_3), 8.55 (ddd, $J_{5,6}$ = 5 Hz, $J_{4,6}$ = 2 Hz, $J_{3,6}$ = 1 Hz, 2H, 2 × pyH_6), 8.12−8.15 (m, 3H, ph $H_{2,4,6}$), 7.90 (dt, $J_{3,4}$ = $J_{4,5}$ = 8 Hz, $J_{4,6}$ = 2 Hz, 2H, 2 × pyH_4), 7.50 (ddd, $J_{4,5}$ = 8 Hz, $J_{5,6}$ = 5 Hz, $J_{3,5}$ = 1 Hz, 2H, 2 × pyH_5).

***N*-phenyl-2-pyridinecarbothioamide.** Distilled aniline (4.68 g, 50.2 mmol), sulfur (4.81 g, 150 mmol), and sodium sulfide nonahydrate (0.240 g, 1.00 mmol) were refluxed in 40 mL of 2-picoline for 30 h. The resulting dark solution was evaporated under reduced pressure, yielding a dark brown oil. This was suspended in water (100 mL), and extracted with DCM (2 × 100 mL). The organic fractions were combined, washed with water (100 mL), dried over $MgSO_4$, and filtered. The DCM solution was reduced in volume to 50 mL and filtered through a short pad of silica, eluting with a further 200 mL of DCM. All volatiles were removed under reduced pressure, and the resulting dark brown oil dried further in vacuo. Crude yield: 9.49 g (88%). A portion of this crude material (2.44 g, 11.4 mmol) was taken up in DCM (20 mL) and again filtered through a short pad of silica, eluted with 100 mL of DCM, yielding a clear orange solution. DCM was removed from this under reduced pressure, and the resulting sticky red-brown oil dried further in vacuo. Cooling in a freezer overnight yielded a red-brown solid. This was taken up in 20 mL of MeOH, filtered while hot to remove any insoluble white water-soluble solid, and then allowed to cool, yielding orange-red crystals. These were isolated by filtration, washed with ice-cold MeOH (10 mL), and thoroughly dried in vacuo. Yield 1.82 g (74% for this purification step, 66% overall). ^{1}H NMR ($CDCl_3$): δ 8.83 (ddd, $J_{3,4}$ = 8 Hz, $J_{3,5}$ = 1 Hz, $J_{3,6}$ = 1 Hz, 2H, 2 × pyH_3), 8.57 (ddd, $J_{5,6}$ = 5 Hz, $J_{4,6}$ = 2 Hz, $J_{3,6}$ = 1 Hz, 2H, 2 × pyH_6), 8.05−8.09 (m, 2H, ph H_3 and H_5), 7.94 (dt, $J_{3,4}$ = $J_{4,5}$ = 8 Hz, $J_{4,6}$ = 2 Hz, 2H, 2 × pyH_4), 7.43−7.54 (m, 3H, 2 × pyH_4, ph H_4), 7.27−7.33 (m, 2H, ph $H_{2,6}$).

4-(3,5-Dichlorophenyl)-3,5-bis(2-pyridyl)-triazole·$^1/_4$H$_2$O (Clbpt). *N*-3,5-dichlorophenyl-2-pyridinecarbothioamide (3.40 g, 12.0 mmol) and 2-pyridinecarbohydrazide (1.97 g, 1.20 mol. equiv) were refluxed in BuOH (50 mL) for 110 h. The dark brown solution was allowed to cool to root temperature (RT), resulting in the formation of fluffly, pale brown crystals. These were isolated by filtration, washed with ice-cold BuOH (30 mL), and dried thoroughly in vacuo. Yield: 2.83 g (64%). $C_{18}H_{11}N_5Cl_2.{}^1/_4H_2O$: calcd C 58.00, H 3.11, N 18.79, Cl 19.02; found C 58.01, H 3.03, N 19.05, Cl 18.99%. ^{1}H NMR ($CDCl_3$): δ 8.36 (ddd, $J_{5,6}$ = 5 Hz, $J_{4,6}$ = 2 Hz, $J_{3,6}$ = 1 Hz, 2H, 2 × py$H_{1/12}$), 8.22 (ddd, $J_{3,4}$ = 8 Hz, $J_{3,5}$ = 1 Hz, $J_{3,6}$ = 1 Hz, 2H, 2 × py$H_{4/9}$), 7.80 (dt, $J_{3,4}$ = $J_{4,5}$ = 8 Hz, $J_{4,6}$ = 2 Hz, 2H, 2 × py$H_{3/10}$), 7.40 (t, J = 2 Hz, 1 H, ph H_{16}), 7.27 (ddd, $J_{4,5}$ = 8 Hz, $J_{5,6}$ = 5 Hz, $J_{3,5}$ = 1 Hz, 2H, 2 × py$H_{2/11}$), 7.20 (d, J = 2 Hz, 2H, ph $H_{14,18}$). ^{13}C NMR ($CDCl_3$): δ 154.1 ($C_{6/7}$), 149.1 ($C_{1/12}$), 146.5 ($C_{5/8}$), 138.7 (C_{13}), 136.8 ($C_{3/10}$), 134.3 ($C_{15/17}$), 128.9 (C_{16}), 127.3 ($C_{14/18}$), 124.4 ($C_{2/11}$), 124.3 ($C_{4/9}$). IR (KBr): ν/cm^{-1} = 3064 (m), 1574 (vs), 1465 (vs), 1449 (vs), 1424 (vs), 1246 (w), 1172 (m), 1137 (m), 1106 (m), 1097 (m), 1044 (w), 1032 (w), 994 (m), 902 (w), 859 (s), 795 (vs), 749 (s), 744 (s), 718 (s), 674 (s), 611 (m), 529 (m), 473 (w), 448 (w), 430 (m). ESI-MS (pos.): m/z = 390.0284 [**Cldpt**·Na]$^+$.

4-Phenyl-3,5-bis(2-pyridyl)-triazole (phbpt). Impure *N*-phenyl-2-pyridinecarbothioamide (1.60 g, 6.60 mmol) and 2-pyridinecarbohydrazide (1.09 g, 1.20 mol. equiv) were refluxed in 50 mL of BuOH for 44 h. The resulting clear, red solution was cooled in a freezer, resulting in the precipitation of a pale orange powder. This was filtered off and washed with BuOH (10 mL), giving a very pale orange powder, which was dried thoroughly in vacuo. Yield: 1.19 g (60%). $C_{18}H_{13}N_5$: calcd C 72.23, H 4.38, N 23.40; found C 72.10, H 4.68, N 23.19%. ^{1}H NMR ($CDCl_3$): δ 8.40 (ddd, $J_{5,6}$ = 5 Hz, $J_{4,6}$ = 2 Hz, $J_{3,6}$ = 1 Hz, 2H, 2 × pyH_6), 8.07 (ddd, $J_{3,4}$ = 8 Hz, $J_{3,5}$ = 1 Hz, $J_{3,6}$ = 1 Hz, 2H, 2 × pyH_3), 7.78 (dt, $J_{3,4}$ = $J_{4,5}$ = 8 Hz, $J_{4,6}$ = 2 Hz, 2H, 2 × pyH_4), 7.34−7.43 (m, 3H, ph H_2, H_4 and H_6), 7.23−7.31 (m, 4H, 2 × pyH_5, ph $H_{3,5}$). ^{13}C NMR ($CDCl_3$): δ 154.5 ($C_{6/7}$), 149.2 ($C_{1/12}$), 147.0 ($C_{5/8}$), 136.7 ($C_{3/10}$), 136.4 (C_{13}), 128.7 (C_{16}), 128.6 ($C_{15/17}$), 128.1 ($C_{14/18}$), 124.7 ($C_{2/11}$), 124.1 ($C_{4/9}$). IR (KBr): ν/cm^{-1} = 1581 (s), 1497 (m), 1462 (s), 1426 (vs), 1174 (m), 1096 (w), 1073 (w), 1046 (w), 1005 (w), 993 (m), 802 (s), 787 (m), 771 (s), 740 (s), 719 (s), 690 (s), 631 (w), 601 (s), 404 (w). ESI-MS (pos.): m/z = 322.1063 [**phdpt**.Na]$^+$

General Procedure for the Synthesis of [Fe(Rdpt)$_3$](BF$_4$)$_2$ (Rdpt = adpt, ibdpt, medpt, pldpt, phdpt, ptdpt, Cldpt, pydpt, or ptmpt). A pale green solution of $Fe(BF_4)_2.6H_2O$ (1 equiv) in acetonitrile (~2 mL) was added dropwise, at ambient temperature, to a stirred colorless solution of the appropriate **Rdpt** ligand (3 equiv) in acetonitrile (5−10 mL) resulting in a deep red solution. After stirring for 2 h, the diffusion of diethyl ether into the reaction solution resulted in the formation of a red crystalline product. Reactions were carried out on scales using 0.07−0.10 mmol of $Fe(BF_4)_2\cdot 6H_2O$.

[Fe(adpt)$_3$](BF$_4$)$_2\cdot 2^1/_3$H$_2$O. A red microcrystalline solid (83%). Found: C, 44.16; H, 3.53; N, 25.27 Calcd for $C_{36}H_{30}N_{18}FeB_2F_8\cdot 2^1/_3H_2O$ (944.20 g mol^{-1}): C, 43.84; H, 3.54; N, 25.56%. IR (KBr): ν/cm^{-1} = 3104 (m), 1634 (m), 1609 (m), 1590 (m), 1521 (w), 1450 (s), 1428 (m), 1291 (w), 1254 (w), 1083 (vs), 1028 (vs), 792 (m), 756 (m), 692 (m), 637 (w), 614 (w), 521 (w), 467 (w). ESI-MS (pos.): m/z = 857.227 [Fe(**adpt**)$_3$](BF$_4$)$^+$.

[Fe(ibdpt)$_3$](BF$_4$)$_2\cdot$H$_2$O. A red crystalline solid (55%). Found: C, 53.05; H, 4.76; N, 19.22. Calcd for $C_{48}H_{51}B_2F_8FeN_{15}\cdot H_2O$ (1085.39 g mol^{-1}): C, 53.11; H, 4.92; N, 19.36%. IR (KBr): ν/cm^{-1} = 3080 (w), 2960 (m), 2874 (w), 1610 (m), 1587 (m), 1521 (m), 1488 (m), 1468 (m), 1449 (s), 1392 (w), 1282 (w), 1245 (w), 1056 (br., vs), 796(m), 747 (m), 713 (m), 690 (w), 600 (w), 520 (m). ESI-MS (pos.): m/z = 980.383 [Fe(**ibdpt**)$_3$](BF$_4$)$^+$.

[Fe(medpt)$_3$](BF$_4$)$_2\cdot 1^1/_2$H$_2$O. A red/orange powder (89%). Found: C, 48.26; H, 3.75; N, 21.70. Calcd for $C_{39}H_{33}N_{15}FeB_2F_8\cdot 1^1/_2H_2O$ (968.25 g mol^{-1}): C, 48.38; H, 3.75; N, 21.70%. IR (KBr): ν/cm^{-1} = 3056 (m), 2958 (m), 1609 (m), 1588 (m), 1529 (m), 1449 (s), 1427 (m), 1372 (w), 1294 (w), 1251 (w), 1083 (vs), 797 (m), 753 (m), 702 (m), 602 (w), 522 (w). ESI-MS (pos.): m/z = 854.242 [Fe(**medpt**)$_3$](BF$_4$)$^+$.

[Fe(pldpt)$_3$](BF$_4$)$_2\cdot 1^1/_2$H$_2$O. A red microcrystalline solid (79%). Found: C, 51.44; H, 3.46; N, 22.45. Calcd. for $C_{48}H_{36}N_{18}FeB_2F_8\cdot 1^1/_2H_2O$ (1119.68 g mol^{-1}): C, 51.41; H, 3.51; N, 22.48%. IR (KBr): ν/cm^{-1} = 3138 (w), 1613 (m), 1586 (m), 1540 (w), 1477 (m), 1449 (s), 1431 (m), 1335 (m), 1286 (w), 1254 (w), 1157 (w), 1083 (vs), 1005 (m), 912 (m), 792 (m), 739 (s), 705 (m), 697 (m), 652 (m), 616 (m), 570 (w), 521 (m). ESI-MS (pos.): m/z = 1007.274 [Fe(**pldpt**)$_3$](BF$_4$)$^+$.

[Fe(phdpt)$_3$](BF$_4$)$_2\cdot$H$_2$O. A red crystalline solid (79%). Found C, 56.81; H, 3.58; N, 18.19. Calcd for $C_{54}H_{39}B_2N_{15}F_8Fe.H_2O$ (1145.47 g mol^{-1}): C, 56.62; H, 3.61; N, 18.34%. IR (KBr): ν/cm^{-1} = 3056 (m), 1609 (w), 1590 (w), 1515 (m), 1497 (m), 1446 (s), 1425 (m), 1362 (w), 1289 (w), 1252 (w), 1083 (br. vs), 1003 (m), 784 (m), 750 (m), 697 (m), 638 (w), 616 (w), 521 (w). ESI-MS (pos.): m/z = 476 [Fe(**phbpt**)$_3$]$^{2+}$.

[Fe(ptdpt)$_3$](BF$_4$)$_2$·2$^1/_2$H$_2$O. A red crystalline solid (72%). Found: C, 56.21; H, 3.95; N, 17.55. Calcd. for $C_{57}H_{45}N_{15}FeB_2F_8 \cdot 2^1/_2H_2O$ (1214.58 g mol^{-1}): C, 56.37; H, 4.15; N, 17.30%. IR (KBr): ν/cm^{-1} = 3081 (w), 1611 (m), 1597 (m), 1514 (s), 1488 (m), 1446 (s), 1425 (m), 1362 (m), 1291 (w), 1255 (w), 1183 (w), 1149 (w), 1054 (br. vs), 1000 (m), 835 (m), 794 (m), 751 (m), 712 (m), 639 (m), 614 (m), 521 (m). ESI-MS (pos.): m/z = 1082.337 [Fe(**ptdpt**)$_3$](BF$_4$)$^+$.

[Fe(Cldpt)$_3$](BF$_4$)$_2$. A red crystalline solid (87%). Found C, 48.89; H, 2.69; N, 15.94. Calcd. for $C_{54}H_{33}B_2Cl_6F_8FeN_{15}$ (1334.13 g mol^{-1}): C, 48.62; H, 2.49; N, 15.75%. IR (KBr): ν/cm^{-1} = 3079 (m), 1610 (w), 1576 (s), 1511 (w), 1486 (m), 1451 (s), 1435 (m), 1285 (w), 1253 (w), 1154 (w), 1054 (br. vs), 994 (m), 865 (w), 810 (w), 793 (m), 743 (w), 711 (w), 793 (m), 743 (w), 711 (w), 686 (m), 618 (w), 521 (w). ESI-MS (pos.): m/z = 579 [Fe(**Clbpt**)$_3$]$^{2+}$.

[Fe(pydpt)$_3$](BF$_4$)$_2$·1$^1/_2$H$_2$O. A red/orange microcrystalline solid (75%). Found: C, 52.93; H, 3.43; N, 21.78. Calcd for $C_{51}H_{36}N_{18}FeB_2F_8 \cdot 2H_2O$ (1157.46 g mol^{-1}): C, 52.92; H, 3.42; N, 21.75%. IR (KBr): ν/cm^{-1} = 3095 (w), 1609 (m), 1586 (s), 1513 (s), 1483 (m), 1447 (s), 1413 (m), 1361 (m), 1291 (w), 1252 (w), 1214 (w), 1177 (w), 1150 (w), 1056 (br. vs), 992 (m), 841 (m), 795 (m), 749 (m), 711 (m), 686 (m), 643 (m), 616 (m), 521 (m). ESI-MS (pos.): m/z = 1043.274 [Fe(**pydpt**)$_3$](BF$_4$)$^+$.

[Fe(ptmpt)$_3$](BF$_4$)$_2$. A red powder (63%). Found: C, 61.54; H, 4.33; N, 14.16. Calcd. for $C_{60}H_{48}N_{12}FeB_2F_8$ (1166.56 g mol^{-1}): C, 61.78; H, 4.15; N, 14.41%. ESI-MS (pos.): m/z = 1079.353 [Fe(**ptmpt**)$_3$](BF$_4$)$^+$.

Computational Studies. The molecular geometries of the eight dipyridyltriazole ligands (Figure 1) were calculated by full geometry optimization with the DFT model B3LYP/6-311G (d,p) with the program Gaussian 03 9.[21] NMR chemical shieldings were computed using these geometries by the GIAO method with the B3LYP/6-311 + G(2d,p) model. ^{15}N chemical shifts were referenced to the shieldings of the nitrogen in nitromethane (at 380 ppm).

Acknowledgment. This work was supported by the University of Otago, including a University of Otago Research Grant (N.G.W. and S.B.). We thank the Tertiary Education Commission (New Zealand) for the award of a Bright Futures Top Achiever Doctoral scholarship to J.A.K. and the MacDiarmid Institute for Advanced Materials and Nanotechnology and the Royal Society of New Zealand Marsden Fund (J.A.K. and S.B.).

Supporting Information Available: Crystallographic data in CIF format, X-ray crystal structure refinement details, perspective views of six of the complexes (Figures S1−S6), details of the packing interactions in the solid state (text and Figures S7−S21), and a table of angles between pyridine and triazole mean planes (Table S1) are provided. The ^{1}H NMR spectra of **pldpt** and [Fe(**pldpt**)$_3$]$^{2+}$ are compared (Figure S22), and VT ^{1}H NMR spectra are provided for the other seven complexes (Figures S23−S31). Figure S32 shows pictures of the calculated geometries for the ligands used in NMR shift calculations. This material is available free of charge via the Internet at http://pubs.acs.org.